Laser Ablation of Copper and YAG:Ce Targets in Liquid PDMS, Studied by Shadowgraph and Photoluminescence Imaging

Rie Tanabe-Yamagishi[*1], Shunsuke Komatsu[1], Yoshiro Ito[2], and Yasutaka Hanada[3]

[1] *Fukuoka Institute of Technology, Japan*
[2] *Nagaoka University of Technology, Japan*
[3] *Hirosaki University, Japan*
[*]*Corresponding author's e-mail: yamagishi@fit.ac.jp*

Laser ablation in liquid (LAL) is a well known metal-nanoparticle generation method. A laser-induced bubble is formed by LAL when the laser is focused on a metal surface immersed in a liquid. Although bubbles produced by the laser ablation in water expand and shrink a few times and then collapse, the bubbles generated on the sample surface in liquid polydimethylsiloxane (PDMS) retain their spherical shape for more than 10 min and can be used to manufacture fine structures via a post-processing method. We observed the process of bubble formation in liquid PDMS using high-speed videography to study the bubble dynamics in detail. When a sintered cerium-doped yttrium aluminum garnet (YAG:Ce) pellet was used as an ablation target, photoluminescence from particles generated by laser ablation was observed under blue-light excitation. A comparison of shadowgraph and photoluminescence images revealed that the laser-induced bubbles were covered with a thin film of polymerized PDMS with YAG:Ce nanoparticles attached. After the polymerized thin film was ruptured, the inner gas-phase bubble floated upward. Light-emitting regions were observed at the film on the target surface and at the bottom of the bubble after the bubble floated upward.
DOI: 10.2961/jlmn.2022.02.2003
Keywords: laser ablation, liquid PDMS, observation, photoluminescence, YAG:Ce particles, laser-induced bubble

1. Introduction

Laser ablation of a metal target immersed in a liquid is one of the methods used to generate metal nanoparticles (NPs), and various studies of laser ablation in a liquid (LAL) have been reported [1-8]. Some measurements and observations have been carried out to elucidate the nature of NPs and their formation mechanisms and dynamics [9-14]. LAL inevitably induces a bubble at the point of laser irradiation, and its dynamical behavior affects the formation process and nature of the NPs [15, 16].

A technique known as microfabrication using laser-induced bubble (microFLIB) has recently been developed. This technique uses bubbles formed during LAL in a liquid thermoset polymer, polydimethylsiloxane (PDMS) [17]. The characteristics of PDMS include high transparency, flexibility, biocompatibility, and low cost, and it is widely used in the fields of biomedical engineering [18-20] and electronic engineering [21]. Whereas a laser-induced bubble generated during laser ablation in water expands and shrinks several times and eventually collapses [15, 16], a bubble generated on a metal surface in liquid PDMS retains its shape and position for more than 10 min. When the laser is scanned along the target surface in liquid PDMS, bubbles are connected to form a tunnel; these bubbles maintain their shape and position for a while. After heat treatment, the tunnel shape is retained in the cured PDMS; thus, the bubbles form a microgroove. In addition, selective metallization by electroless plating is only possible in the microgroove area on PDMS, which suggests that a plasma plume that includes metal particles is generated by laser ablation and that the metal particles remain on the inside surface of the bubble tunnel to act as seeds for the plating process.

In this research, we address the following two questions: First, why does the bubble induced by LAL in liquid PDMS maintain its shape and position for an extended period? Second, how do metal particles form during LAL? To answer these questions, we have attempted to observe the ablation phenomenon directly. Shadowgraph imaging is one of the observation methods commonly used to examine the laser ablation phenomenon [22-24], and photoluminescence imaging is a powerful tool for detecting NPs produced in LAL when a fluorescent target is used [25]. We speculated that these two imaging methods that employ a high-speed camera can be used to clarify the aforementioned issues. In the present work, shadowgraph images are recorded for a copper target and shadowgraph and photoluminescence images are recorded for both a copper target and a fluorescent sintered cerium-doped yttrium aluminum garnet (YAG:Ce) target in liquid PDMS. The obtained images are then compared to examine the dynamical changes of the laser-induced bubbles on both targets and the distribution of NPs generated by laser ablation in liquid PDMS.

2. Experimental setup

Liquid PDMS was mixed with a curing agent at a mass ratio of 10:1. A copper block or a sintered YAG:Ce pellet was used as a target, and the target was immersed in liquid PDMS to a depth of 2 mm. YAG:Ce is a yellow-emitting phosphor under blue-light excitation and is used in white LEDs in combination with blue-LED excitation [26].

YAG:Ce powder was pressed into a 10 mm-diameter pellet and sintered at 1500 °C for 8 h under a N_2 atmosphere to prevent the oxidation of Ce^{3+} to Ce^{4+}.

Figure 1 shows a schematic of the shadowgraph imaging method. A single pulse at 532 nm from a nanosecond Nd:YAG laser was used as an ablation pulse, and a continuous-wave (CW) laser at 532 nm was used as an illuminating light source for a high-speed video camera. The energy of the ablation pulse was measured and adjusted in front of the objective lens. A band-pass filter at 532 nm was installed in front of the camera to avoid halation by the ablation plasma. Shadowgraph movies were recorded at 60 frames per second (fps) with a shutter speed of 1/178,000 s.

Figure 2 shows a schematic of the photoluminescence imaging method. A CW laser at 477 nm was used as the excitation light for YAG:Ce. In this observation, backlight illumination and filters were not used. Because the observation interval was 16 ms, the cut of plasma induced by the ablation laser of a pulse width of 10 ns was not a concern. For the excitation laser at 477 nm, although reflecting spots from the bubble surface appeared in the image, they did not interfere with observations of the NP distribution. Photoluminescence movies were recorded at 60 fps with a shutter speed of 1/50,000 s. The images were acquired with a resolution of approximately 2.2 μm per pixel.

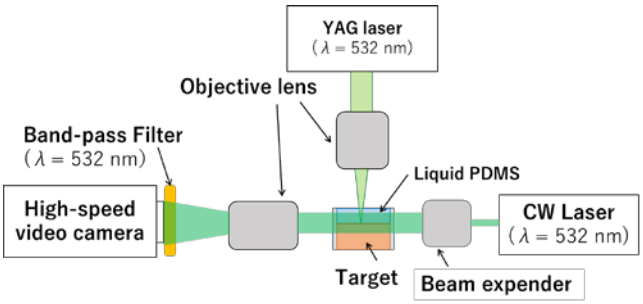

Fig. 1 Schematic of shadowgraph imaging.

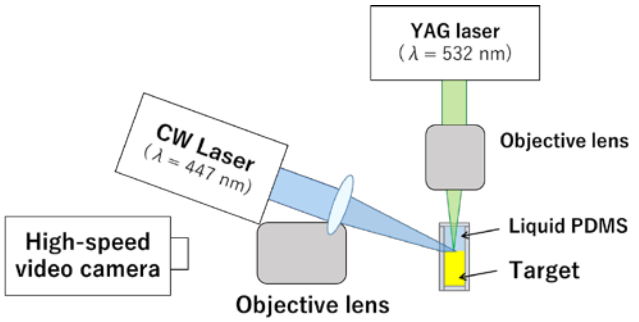

Fig. 2 Schematic of photoluminescence imaging.

3. Results and discussion

To examine bubble behavior during pulse laser irradiation of the copper target in liquid PDMS, high-speed video imaging was carried out in shadowgraph mode. Figure 3 shows shadowgraph images extracted from a video of the laser ablation process in liquid PDMS, where the laser energy was 0.5 mJ. The recording speed was 60 fps and the video was recorded until 1048 s after the laser pulse irradiation. A copper block that used in previous microFLIB experiments [17] was selected as a target metal. The black horizontal shadow that appears at the bottom of each image is the copper target. The copper surface was irradiated with a single laser pulse. After laser irradiation, a slightly ellipsoidal bubble was formed on the copper surface. The gas inside the bubble likely consisted of vapors from the target and the decomposition products of PDMS. The bubble is considered to be covered by a spherical balloon composed of polymerized PDMS. PDMS is polymerized quite easily by heating [17]; thus, heating of the target by laser irradiation and by the gas in the bubble caused the PDMS at the bubble surface to polymerize to form a balloon. The bubble gradually became spherical over a period of a few seconds. The bubble retained its shape and position for more than 100 s, with a slight increase in its radius.

Some strings and membranes (hereafter, "strings" for simplicity) connecting the lower part of the bubble and the metal surface appeared, as indicated by arrows in Figure 3. The bubble finally detached from the copper surface and floated upward. The formation of connecting strings might explain why the bubbles remained on the metal plate for more than 10 min. We speculate that the shadows of these strings show polymerized PDMS formed by rapid local heating due to laser ablation of the metal. In the microFLIB process, bubbles are formed successively in short intervals (less than 1 ms) on the copper surface. With laser scanning, they reside on the surface and connect continuously to form a tunnel. Upon heat treatment, the bubble tunnel is converted to a permanent structure [17].

Figure 4 shows shadowgraph images extracted from a video of laser ablation of the YAG:Ce target in liquid PDMS with a laser pulse energy of 0.5 mJ. The video was recorded at 60 fps, and was recorded as a single movie until 1140 s after laser pulse irradiation. The image at 1600 s was taken as the final state. Although the target surface was polished with 1000 grit sandpaper, the surface was not as flat as that of the copper target. The first frame of the video was recorded 16 ms after laser irradiation, and the laser-induced bubble was slightly ellipsoidal. The bubble gradually became spherical and retained its shape and position for more than 100 s, which is the same behavior observed when a copper target was used. The diameter of the bubble increased with time and was approximately 270 μm at 500 s. Thereafter, the bubble gradually floated upward, leaving strings on the target surface. Although the time at which the bubble started to float varied with each shot, the phenomenon observed during single-shot irradiation in liquid PDMS was approximately the same irrespective of the target material.

Photoluminescence images were recorded at 60 fps, and some selected images are shown in Figure 5. In these images, particles of YAG:Ce are observed as white, cloudy regions inside the bubble. White spots with sizes of a few tens of micrometers in the middle region of the bubble are reflections of the excitation light from the bubble surface. The first image obtained at 16 ms shows that the bubble shape and size are approximately the same as those for the bubble observed in the shadowgraph image in Figure 4 and that the entire bubble appears to emit light. The light-emitting region occupied the entire bubble until ~283 s. The horizontal size of the bubble was approximately 224 μm at 5 s and 252 μm at 200 s. Although it was difficult to observe the bubble edge after the light-emitting region disappeared from the bubble top, it was more clearly observed

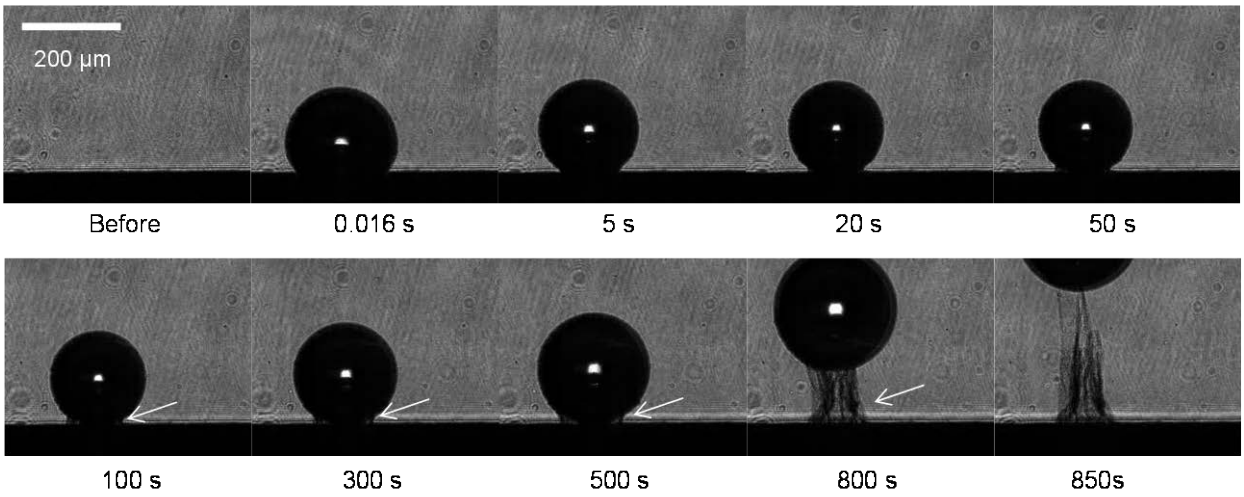

Fig. 3 Shadowgraph images extracted from video recorded at 60 fps for 0.5 mJ pulse. The time resolution of the shadowgraph images is 1/178,000 s. The target is a copper plate.

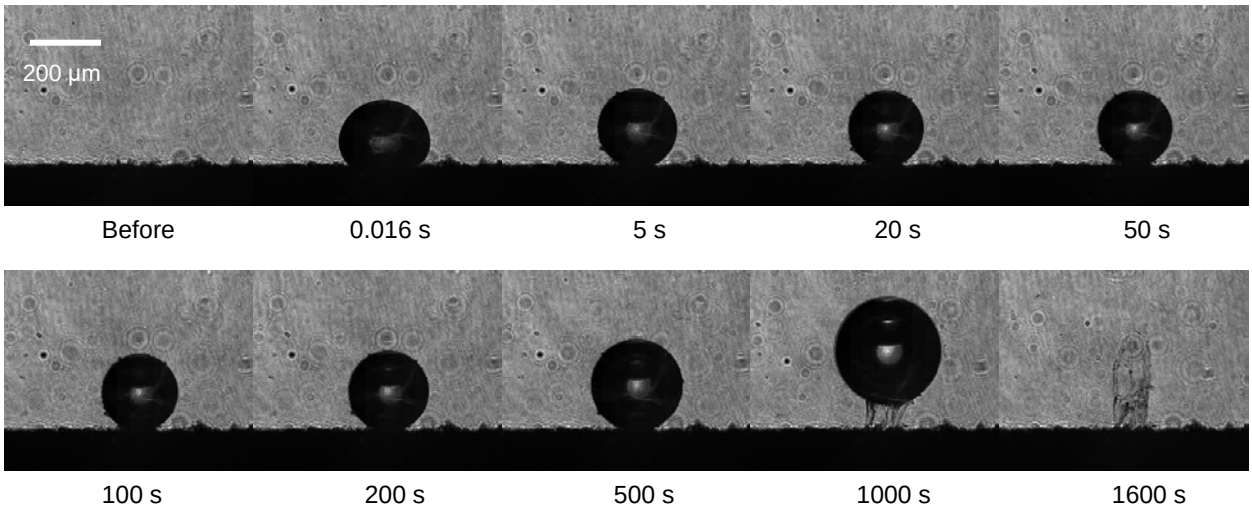

Fig. 4 Shadowgraph images extracted from video recorded at 60 fps for 0.5 mJ pulse. The time resolution of the shadowgraph images is 1/178,000 s. The target is sintered YAG:Ce.

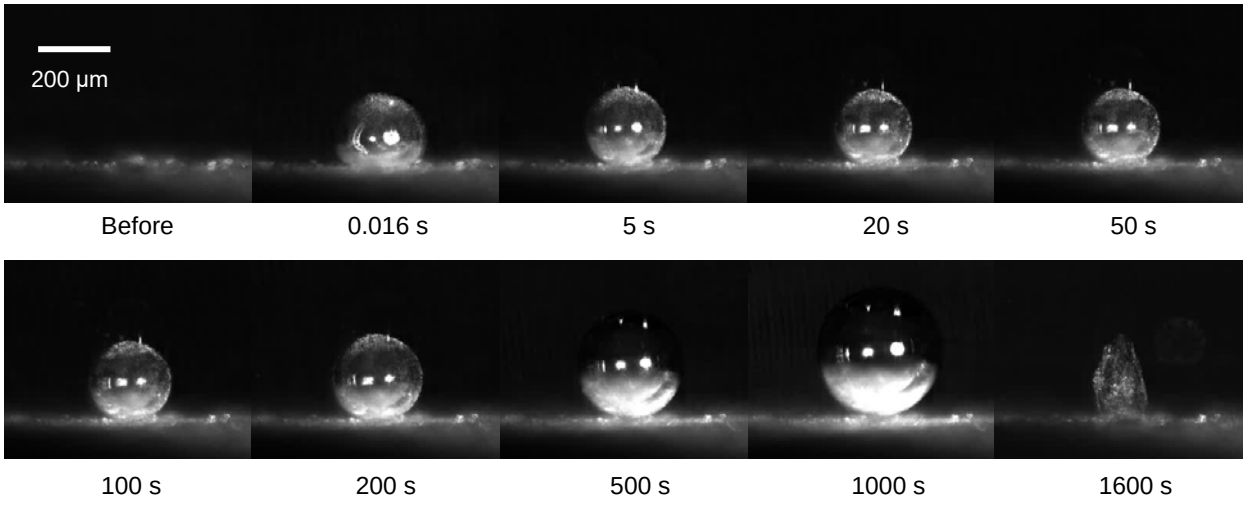

Fig. 5 Photoluminescence images extracted from video recorded at 60 fps for 0.5 mJ pulse. The time resolution of the shadowgraph images is 1/50,000 s. The target is sintered YAG:Ce.

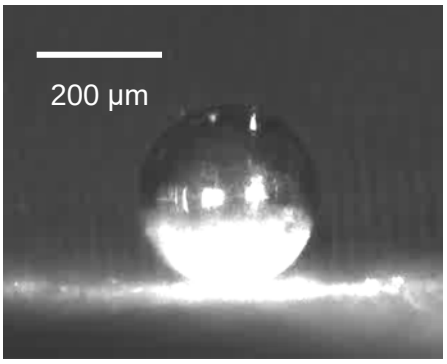

Fig. 6 Photoluminescence image at 400 s after brightness and contrast were adjusted to enable clear observation of bubble edge.

Fig. 7 Photoluminescence images at 280, 350, and 450 s. The solid line shows the outer edge of the bubble, and the dashed line shows the outer edge of the light-emitting region.

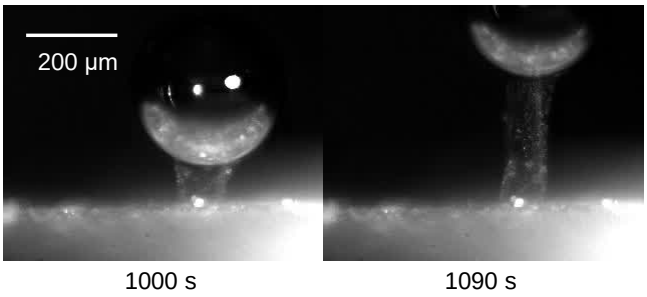

Fig. 8 Photoluminescence images at 1000 and 1090 s. These images are obtained after different laser shots than those corresponding to the images in Figures 5 to 7.

after the brightness and contrast of the image were adjusted (Figure 6). The emitting region began to detach from the upper part of the bubble and gathered toward the lower part while the laser-induced bubble continued to expand (Figure 7). The solid lines in Fig. 7 show the outer edge of the bubble, and the dashed lines show the outer edge of the light-emitting region. The horizontal size of the bubble was approximately 308 μm at 500 s, and the bubble subsequently expanded to 352 μm at 1000 s. At ~1000 s or later, the bubble started to float upward; as shown in Figure 8, the light-emitting area at the bottom of the bubble became narrower and dimmer. The light-emitting area that detached from the boundary of the bubble always appeared in the lower part of the bubble, and the strings and membranes formed a columnar structure that remained on the target surface as the bubble floated upward. We considered that the bubble formed by LAL in liquid PDMS was covered with a balloon composed of a polymerized PDMS thin film, and that polymerization would eventually stop when the gas was cooled. However, the expansion of the inner gas-phase bubble continued such that the balloon formed and only the gas bubble floated upward. Thus, the gas-phase bubble separated from the polymerized PDMS and the columnar residues of the polymerized PDMS balloon and strings attached to the target surface were observed in both the shadowgraph and photoluminescence images. The location and timing of this rupture were inconsistent. Columnar images were obtained by photoluminescence imaging, suggesting that the NPs of YAG:Ce were adhered to the columnar structures. Because the light-emitting regions remained at the bottom of the bubble as the bubble floated upward, we considered that most of the NPs produced by laser ablation were confined inside the bubble, likely at the bubble–liquid interface.

From these photoluminescence observations, we conclude that the laser-induced bubble is covered with a balloon composed of a thin film of polymerized PDMS and that the YAG:Ce particles are contained inside the bubble, many of them attached to the inner surface of the balloon. The polymerized PDMS thin film splits because of the growth of the bubble, and the film then gathers onto the bubble bottom on the target surface. Because the light emission at the bottom of the bubble continues even after the bubble floats upward (Figure 8), we consider that most of the NPs produced by laser ablation are confined inside the bubble. These results are consistent with our previously reported finding that NPs formed by LAL are confined in the laser-induced bubble [25]. In addition, the findings of the present study support our previous results showing that the microtunnels formed by connected microbubbles after thermal treatment of PDMS were successfully and selectively metalized by plating [17]; copper NPs formed by LAL adhered onto the surface of the tunnel structure and acted as seeds for the plating of a metal onto the polymer.

4. Summary

To examine the dynamics of laser-induced bubbles and the process of NP formation during laser ablation in liquid PDMS, we observed laser ablation in liquid PDMS via shadowgraph and photoluminescence imaging using a high-speed video camera. Shadowgraph movies showed the existence of strings or membrane-like shadows between the bottom of the bubble and the surface of the target in a time period starting a few seconds after laser irradiation. We propose that the strings/membranes are polymerized PDMS resulting from local heating at the boundary of the target surface and liquid PDMS and they bind the bubble to the target surface. Photoluminescence images of the YAG:Ce NPs formed by LAL were successfully obtained and revealed that the laser-induced bubble was covered with a balloon composed of a thin film of PDMS with attached YAG:Ce NPs. The balloon was ruptured by the expansion of the inner gas-phase bubble, and then only the gas-phase bubble floated upward, leaving the raptured balloon and strings on the target surface. Light-emitting regions at the bottom of the bubble were observed even after the bubble floated upward. From these observations, we conclude that localized polymerization that occurs during LAL in liquid PDMS is why the laser-induced bubble remains on the target surface for more than 10 min and why some of the NPs fabricated by LAL are attached to the polymerized thin film, whereas others are trapped inside the gas-phase bubble.

Acknowledgments
This work was supported by a JSPS KAKENHI Grant-in-Aid for Scientific Research (Grant Number: 20H02646). The authors thank Prof. H. Wada of Tokyo Institute of Technology for providing the YAG:Ce pellet.

References

[1] F. Mafuné, J. Kohno, Y. Takeda T. Kondow, and H. Sawabe, J. Phys. Chem. B,104, (2000) 8333.
[2] F. Mafuné, J. Kohno, Y. Takeda T. Kondow, and H. Sawabe, J. Phys. Chem. B, 104, (2000) 9111.
[3] H. Usui, Y. Shimizu, T. Sasaki, and N. Koshizaki, J. Phys. Chem. B, 109, (2005) 120.
[4] U. Taylar, S. Klein, S. Petersen, W. Kues, S. Barcikowski, and D. Rath, Cytometry A, 77A, (2010) 439.
[5] H. Wang, O. Odawara, and H. Wada, J. Alloys Compd., 683, (2016) 1.
[6] D. Zhang, B. Gökce, C. Notthoff and S. Barcikowski, Sci. Rep., 5, (2015) 13661.
[7] D. Zhang, B. Gökce, and S. Barcikowski, Chem. Rev., 117, (2017) 3990.
[8] H. Wang, M. Lau, T. Sannomiya, B. Gökce, S. Barcikowski, O. Odawara, and H. Wada, RSC Adv., 7, (2017) 9002.
[9] T. Tuji, Y. Okazaki, Y. Tsuboi, and M. Tuji, Jpn. J. Appl. Phys., 46, (2007) 1533.
[10] W. Soliman, N. Takada, and K. Sasaki, Appl. Phys. Express, 3, (2010) 035201.
[11] P. Wagener, S. Ibrahimkutty, A Menzel, A. Plech, and S. Barcikowski, Phys. Chem. Chem. Phys., 15, (2013) 3068.
[12] A. Matsumoto, A. Tamura, T. Honda, T. Hirota, K. Kobayashi, S. Katakura, N. Nishi, K. Amano, K. Fukami, and T. Sakka, J. Phys. Chem. C, 119, (2015) 26506.
[13] J. Lam, J. Lombard, C. Dujardin, G. Ledoux, S. Merabia, and D. Amans, Appl. Phys. Lett., 108, (2016) 074104.
[14] S. Reich, P. Schönfeld, P. Wagener, A. Letzel, S. Ibrahimkutty, B. Gökce, S. Barcikowski, A. Menzel, T. Santos Rolo, A. Plech, J. Colloid Interface Sci., 489, (2017) 106.
[15] R. Tanabe, T. T. P. Nguyen, T. Sugiura, and Y. Ito, Appl. Surf. Sci., 351, (2015) 327.
[16] S. Kohsakowski, B. Gökce, R. Tanabe, P. Wagener, A. Plech, Y. Ito, and S. Barcikowski, Phys. Chem. Chem. Phys., 18, (2016) 16585.
[17] T. Naruse and Y. Hanada, Opt. Express, 27, (2019) 9429.
[18] S. Torino, B. Corrado, N. Iodice, and G. Coppola, Inventions, 3, (2018) 65.
[19] I. Miranda, A. Souza, P. Sousa, J. Ribeiro, E. M. S. Castanheira, R. Lima, and G. Minas, J. Funct. Biomater., 13 (2022) 2.
[20] E. Pedraza, A. Brady, C. A. Fraker, and C. L. Stabler, J. Biomater. Sci. Polym. Ed., 24, (2013) 1041.
[21] S. Hayashi, Y. Nakajima, and M. Terakawa, Opt. Mater. Express, 9, (2019) 2672.
[22] A. Vogel, S. Busch and M. Asiyo-Vogel, SPIE Vol.1877, Ophthalmic Technologies III, (1993) 312.
[23] Y. Ito, Proc. SPIE 6106, (2006) 61060T.
[24] H. Ohba, M. Saeki, I. Wakaida, R. Tanabe, and Y. Ito, Opt. Express, 22, (2014) 24478.
[25] R. Tanabe-Yamagishi, Y. Ito, H. Wang, and H. Wada, Appl. Phys. Express., 13, (2020) 075008.
[26] N. Tsuruoka, T. Sasagawa, T. Yodo, M. Yoshimoto, O. Odawara, and H. Wada, SpringerPlus, 5, (2016) 325.

(Received: June 3, 2022, Accepted: August 28, 2022)